Tuijin Jishu/Journal of Propulsion Technology
ISSN: 1001-4055
Vol. 46 No. 2 (2025)

Mathematical Modeling and Stability Analysis of an Electric Propulsion System with Energy Recovery Mechanism

G. Santhosh Kumar and M. Aakash*

Department of Mathematics, Easwari Engineering College, Ramapuram, Chennai – 600089, Tamil Nadu.

Department of Mathematics, Jeppiaar Engineering College, Jeppiaar Nagar, Chennai – 600119, Tamil Nadu.

Abstract:- Electric propulsion systems have revolutionized transportation by increas ing efficiency, energy efficiency, and environmental sustainability. In this study, we analyze a propulsion system comprised of a DC motor, a battery pack, and a su percapacitor pack, which are integrated through bidirectional and boost converters. In order to characterize the interaction among these components, a mathematical model is developed that incorporates both electrical and mechanical dynamics. An equilibrium point is used to evaluate the response of a system to perturbations, while a Jacobian matrix is used to evaluate its response to changes. An analysis of the eigenvalues and Bode plots of the proposed system is carried out to evaluate its sta bility and efficiency. These findings provide valuable insights into optimizing energy transfer, improving power management, and ensuring reliable performance in electric vehicle applications. As a result of this research, advanced propulsion systems will be developed, leading to innovation in sustainable energy solutions.

Keywords*: Mathematical Modeling, Stability analysis, Electric Propulsion, Numerical simulation, Non linear Differential equations.*

1. Introduction

The modeling [1] and simulation of propulsion systems, electric motors, and intelligent motion control play a pivotal role in the design process. Currently, various propulsion solutions are being developed, including synchronous motors powered by power electronics-based inverters and DC motors utilizing batteries and supercapacitors for energy supply and recovery. The proposed energy supply and recovery system comprises a DC motor, a battery, and a supercapacitor pack specifically designed for electric vehicle propulsion. Previous research has optimized electrical configurations for such systems using DC motors [2], [3] and [4]. This study explores new aspects of system architecture and investigates optimization possibilities based on the electrical models of system components. Each component is mathematically modeled to construct a comprehensive system model, with simulations conducted to identify stability conditions necessary for implementing control strategies that enhance system performance.

Electric propulsion systems offer significant advantages for various ship applica tions with variable velocity profiles, such as supply vessels, floating production units, drill ships, shuttle tankers, icebreakers, naval ships, and cruise liners. Prior studies provide detailed insights into configurations, applications, maintenance procedures, safety protocols, and class regulations. The core concept of these systems involves replacing conventional diesel propulsion engines with electric motors and distribut ing power generation across multiple smaller diesel generators. Unlike diesel engines, which achieve peak efficiency only at their nominal operating points, electric motors maintain high efficiency across a broad range of speeds and power outputs. Ships with variable velocity requirements can sustain efficiency by adjusting the number of active diesel generators based on power demand, unlike traditional diesel propulsion systems that experience significant efficiency losses outside their optimal

range. Additional benefits of these systems are discussed later in the study. The modeling of diesel-electric propulsion (DEP) systems is driven by the need to simulate various scenarios to assess performance and ensure electrical network stability. Another objective is to advance Power Management Systems (PMS) through sophisticated control algorithms that optimize fuel usage and improve safety [5] and [6]. Optimization methods determine the ideal number of generators and load-sharing strategies, while handling significant load variations may require advanced control techniques and non-linear mathematical models expressed in compact vector forms.

This study integrates well-established models of individual components to create an interconnected system that operates without an infinite bus. A dynamic model for power generation and static models for thruster drives are presented. PID controllers are used to represent speed governors and Automatic Voltage Regulators (AVRs), and the entire system is described using a non-linear state-space framework suitable for simulation and control design [20].

2. Systematic assessment of an elements

In combination, the battery pack and supercapacitor pack in the system design pro vide the power and energy needed by the system load, which is a DC motor. A bidirectional converter and a boost converter are part of the control system. The complete system design is shown in Figure 1. A steady voltage is supplied to the DC electric motor's input by the battery (SB). During the traction phase, the boost converter (CB) only uses step-up mode to raise the battery voltage to what the DC motor needs. Power transfer to and from the supercapacitors is facilitated by the bidirectional converter (CBD), which operates in step-down mode during the braking phase and step-up mode during the traction phase. The supercapacitor pack (SC) recovers energy during braking and provides peak power at times of high demand. This reversible converter is necessary for the supercapacitors' charge and discharge processes. The DC motor has a good torque curve at low speeds, making it ideal for the needs of electric cars [7]. An ideal passive component coupled in series with a resistance is used to represent the supercapacitor pack.

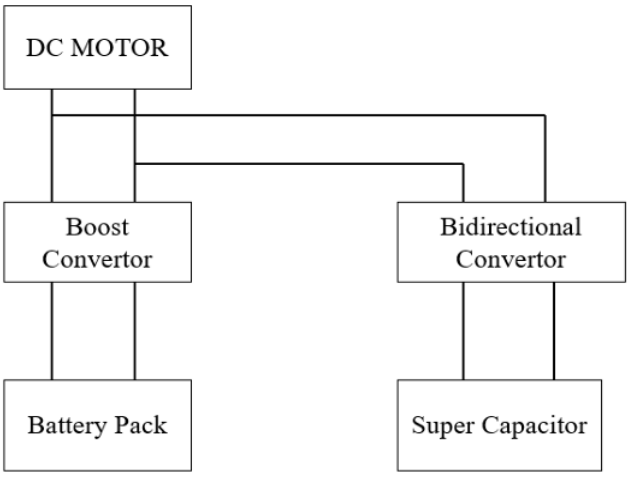

Figure 2.1: The architecture of a propulsion system incorporating a DC motor

The interactions between the DC bus and the supercapacitors are captured in the mathematical model of the buck-boost converter and supercapacitor pack system. The mathematical model that illustrates the DC motor's operation includes both mechanical and electrical equa tions that define its linear behaviour. Figure 2.2 provides a detailed equivalent circuit representation of a battery pack, which is a fundamental component in energy supply systems for propulsion. The circuit consists of two primary elements: an ideal voltage source β1 and an internal series resistance α. The ideal voltage source models the open-circuit voltage of the battery, representing the theoretical maximum voltage it can provide under no-load conditions. This voltage remains constant and indepen dent of the

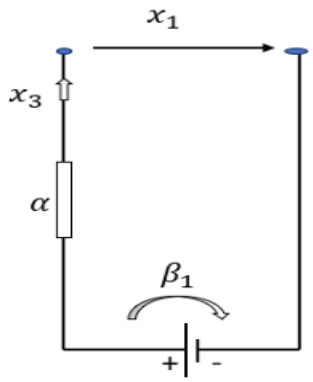

Figure 2.2: The equivalent circuit representation of the battery pack

external load, making it a simplified abstraction of the battery's chemical potential. The internal series resistance α accounts for the real-world losses that oc cur within the battery due to its internal electrochemical and material properties. These losses manifest as a voltage drop across the resistance when current x3 flows through the circuit. Consequently, the terminal voltage x1, which is the voltage avail able to the external load, is affected by the internal resistance and is given by the equation x1 = β1 − αx3.This relationship shows that the terminal voltage decreases with increasing current due to the resistive losses.

This equivalent circuit model is widely used in system-level simulations because of its simplicity and effectiveness in capturing the essential behavior of a battery [8]. It enables the analysis of power delivery, energy efficiency, and voltage fluctuations when the battery interacts with other components, such as DC motors or converters. By incorporating this model into the larger propulsion system, engineers can predict the battery's performance under various operational scenarios and optimize the system's overall efficiency and stability. Figure 2.3 depicts the equivalent circuit representation of a DC motor, designed to capture its electrical behavior in propulsion systems. The circuit consists of a supply voltage x9, a series resistance ϕ, an inductance γ3, and an electromotive voltage kω. The resistance ϕ accounts for the energy losses due to the motor's internal wiring and components, while the inductance γ3 represents the energy stored in the motor's magnetic field during operation. The electromotive volt age kω, often referred to as back-EMF, is proportional to the motor's angular speed and opposes the applied voltage, reflecting the motor's dynamic response. The rela tionship between these components is governed by Kirchhoff's voltage law, where the supply voltage is distributed across the resistance, inductance, and back-EMF.

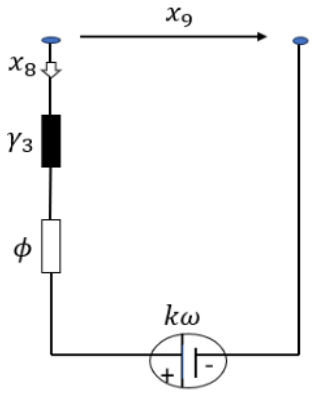

Figure 2.3: The equivalent circuit representation of the DC motor

This model serves as a foundation for analyzing the motor's performance under varying electrical and mechanical conditions, enabling its integration into larger propulsion and energy management systems. Figure 2.4 provides the Laplace representation of the DC motor's equivalent model, which is a fundamental tool for analyzing and designing propulsion systems. This model uses transfer functions to represent the dynamic relationship between the input voltage and the motor's speed or torque, offering a mathematical framework to study its behavior under

various operational conditions. Key components of the DC motor, such as resistance, inductance, and back electromotive force (EMF), are included in the model to capture the electrical and mechanical interactions accurately [11].

The resistance represents energy losses due to the internal wiring and other elec trical components, while the inductance reflects the energy stored in the motor's magnetic field during operation. The back EMF, which is proportional to the mo tor's angular velocity, opposes the applied voltage and illustrates the motor's dynamic response. These elements interact according to Kirchhoff's voltage law, which governs the distribution of the input voltage across the motor's electrical components [12].

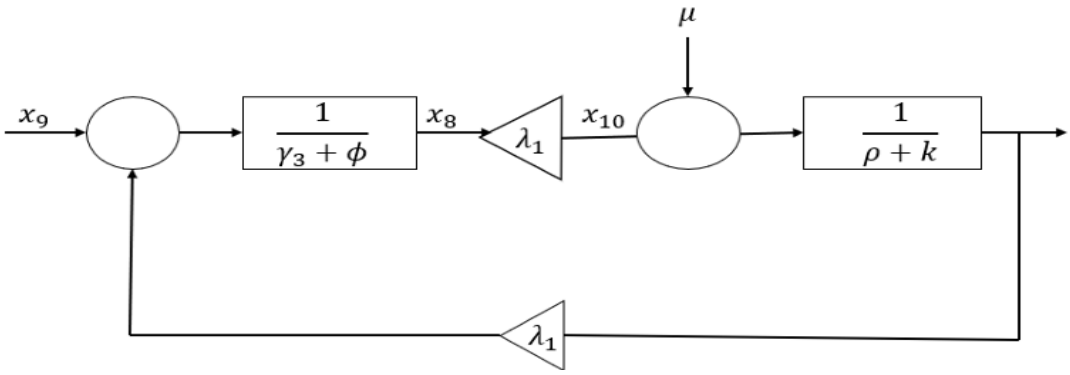

Figure 2.4: The Laplace representation of the DC motor's equivalent model.

The Laplace domain simplifies these complex time-domain interactions into al gebraic equations, enabling easier analysis and design of control systems. Engineers use this representation to predict the motor's response to input variations, design control strategies for stability, and optimize performance. By integrating this model into larger propulsion and energy management systems, designers can simulate var ious operational scenarios, identify potential issues, and implement solutions that enhance overall efficiency and reliability. This approach is particularly important in systems where precise control of motor dynamics is critical, such as electric vehicles or advanced propulsion systems [13].

3. The Proposed Model

The mathematical model [9] and [10] of the overall system, instrumental in the stability analysis of the propulsion, supply, and recovery system featuring a DC motor, is expressed through a set of equations. These equations systematically represent the dynamic interactions and operational characteristics of the system components. The model encompasses both electrical and mechanical domains, integrating parameters such as the DC motor's resistance, inductance, back electromotive force (EMF), and torque. This representation facilitates a detailed investigation of system behavior under varying conditions, enabling precise stability analysis. By incorporating the interde pendencies between the battery pack, supercapacitor pack, bidirectional converters, and the DC motor, the equations describe energy transfer and recovery processes during traction and braking phases. Furthermore, the model is pivotal for predicting the system's response to control inputs, external disturbances, and operational load variations.

Through this formalized mathematical framework, engineers are equipped to eval uate the performance, identify stability margins, and optimize control strategies for the propulsion system. This systematic approach ensures the reliable operation of the DC motor in diverse applications, such as electric vehicles and advanced energy management systems, while also enhancing energy efficiency and overall system ro bustness.

$$\alpha\beta_1 x_1 - x_2 = 0,$$

$$\gamma_1 x_2 - (1 - \delta_1)\gamma_2 x_3 = 0,$$

$$\delta_2 x_3 + (1 - \epsilon)x_4 - \eta x_5 = 0,$$

$$\gamma_3 x_4 - x_5\phi = 0,$$
$$x_6 + (1-\zeta)\psi x_7 - \rho x_8 = 0,$$
$$x_7\gamma + \sigma = 0,$$
$$\lambda_1 x_8 - \lambda_2 \omega x_9 = 0,$$
$$x_9\theta + k\mu = 0.$$

The dynamic interactions within the propulsion system are represented by the me chanical interpretation of the model, which focuses on motion control, torque produc tion, and energy transfer. The interactions between mechanical parts, including the DC motor's rotational dynamics, the effects of torque, friction, and inertia, and the impact of electrical inputs on mechanical outputs, are described by the variables and parameters. This framework makes it possible to forecast how the system will behave under various load and speed scenarios, which makes stability analysis and mechani cal performance improvement easier in applications like energy recovery systems and electric cars.

Table:1. Detailed descriptions of the system's parameters

Parameter	Description
x_1	Battery Voltage
α	Battery Resistance
x_3	Battery current
γ_1	Battery Inductance
x_5	Supercapacitor Voltage
ϕ	Supercapacitor resistance
x_4	DC bus voltage
η	DC bus capacitance
δ_1	Boost convertor duty cycle
ζ	Bidirectional convertor duty cycle
γ_3	Motor Inductance
ϕ	Motor Resistance
ω	Motor angular speed
x_9	Motor voltage
x_8	Motor current
k	Viscous friction coefficient
μ	Resistant torque

4. Stability Analysis of the Electric Propulsion System Model

The objective of this research is to determine if the stability of this system can be determined through the analysis of equilibrium points and the assessment of how those equilibrium points respond to perturbations. An equilibrium state occurs when a dynamical system reaches a steady-state condition, which implies that all time derivatives of the state variables are zero. As a result, the state variables do not change over time, and the rate of variation of

each state variable falls. Let $x^* = (x_1^*, x_2^*, x_3^*, \dots, x_9^*)$ represent the equilibrium state of the system, where each x_i^* (for $i = 1,2, \dots,9$) denotes the steady-state value of the corresponding state variable x_i. The equilibrium state satisfies the condition that when the time derivatives of all governing differential equations become zero, they become algebraic equations [14], [16] and [17]. When a differential equation's time derivative is zero, all governing differential equations reduce to algebraic equations. According to mathematics, if a set of ordi nary differential equations of first order of the form governs the system,

$$\frac{dx_i}{dt} = f_i(x_1, x_2, \dots, x_9), \text{ for } i = 1,2, \dots,9 \qquad (4.1)$$

then, at equilibrium, we impose the steady-state condition, $\frac{dx_i}{dt} = 0$, for all i. By setting the left-hand sides of these equations to zero, we obtain a system of nonlinear algebraic equations, $f_i(x_1, x_2 \dots x_9) = 0$ for $i = 1,2, \dots,9$. As a result of solving this system, we obtain the equilibrium values A, which determine the state at which the system remains unchanged over time. Analysis of the stability of this equilibrium can be conducted by considering the eigenvalues of the Jacobi an matrix of the system, but this step goes beyond just identifying the equilibrium state. Thus, the equilibrium solution is obtained by solving the algebraic equations resulting from the steady-state condition, which provide the values at which the system maintains a constant state over time $x_2^* = \alpha\beta_1 x_1$, $x_3^* = \frac{\gamma_1 x_2^*}{(1-\delta_1)\gamma_2}$, $x_4^* = \frac{\delta_2 x_3^* + \eta x_5^*}{(1-\epsilon)}$, $x_5^* = \frac{\gamma_3 x_4^*}{\phi}$, $x_6^* = \frac{-\sigma}{\nu}$, $x_7^* = \frac{\rho x_6^* + (1-\zeta)\psi x_7^*}{\rho}$, $x_8^* = \frac{\lambda_1 x_8^*}{\lambda_2 \omega}$, $x_9^* = \frac{-k\mu}{\theta}$. This gives the steady-state solutions in terms of system parameters. To analyze stability, we linearize the system by computing the Jacobian matrix,

$$J = \begin{pmatrix} \frac{\partial f_1}{\partial x_1} & \frac{\partial f_1}{\partial x_2} & \dots & \frac{\partial f_1}{\partial x_9} \\ \dots & \dots & \dots & \dots \\ \frac{\partial f_9}{\partial x_1} & \frac{\partial f_9}{\partial x_2} & \dots & \frac{\partial f_9}{\partial x_9} \end{pmatrix}$$

Substituting the given equations, we derive

$$J = \begin{pmatrix} \alpha\beta_1 & -1 & 0 & 0 & 0 & 0 & 0 & 0 & 0 \\ 0 & \gamma_1 & -(1-\delta_1)\gamma_2 & 0 & 0 & 0 & 0 & 0 & 0 \\ 0 & 0 & \delta_2 & (1-\epsilon) & -\eta & 0 & 0 & 0 & 0 \\ 0 & 0 & 0 & \gamma_3 & -\phi & 0 & 0 & 0 & 0 \\ 0 & 0 & 0 & 0 & 0 & 1 & (1-\zeta)\psi & -\rho & 0 \\ 0 & 0 & 0 & 0 & 0 & 0 & \nu & 0 & 0 \\ 0 & 0 & 0 & 0 & 0 & 0 & 0 & \lambda_1 & -\lambda_2\omega \\ 0 & 0 & 0 & 0 & 0 & 0 & 0 & 0 & \theta. \end{pmatrix},$$

The stability of a dynamical system at equilibrium is determined by analyzing the eigenvalues of the Jacobian matrix, denoted as J. The Jacobian matrix is a fundamental tool instability analysis and is defined as the matrix of first-order partial derivatives of the system of equations governing the dynamics. Mathematically, if the system is described by a set of first-order differential equations,

$$\frac{dx_i}{dt} = f_i(x_1, x_2, \dots, x_n), \text{ for } i = 1,2,3, \dots n. \qquad (4.2)$$

Then the Jacobian matrix J is given by,

$$J = \begin{pmatrix} \frac{\partial f_1}{\partial x_1} & \frac{\partial f_1}{\partial x_2} & \dots & \frac{\partial f_1}{\partial x_9} \\ \dots & \dots & \dots & \dots \\ \frac{\partial f_n}{\partial x_1} & \frac{\partial f_n}{\partial x_2} & \dots & \frac{\partial f_n}{\partial x_n} \end{pmatrix},$$

Evaluating J at the equilibrium point x^* denoted as $J(x)$, provides insight into the system's local behavior near ∏equilibrium. To determine stability, we analyze the eigen values λ_i of $J(x^*)$, which satisfy the characteristic equation, $\det(\lambda - JI) = 0$. The equilibrium is classified based on the real parts of these eigenvalues. If all eigenvalues λ_i have negative real parts, $Re(\lambda_i) < 0$ for all i, then perturbations around the equilibrium decay over time, and the equilibrium is said to be locally stable (asymptotically stable). If at least one eigenvalue has a positive real part, i.e., $Re(\lambda_i) > 0$ for some i, then small perturbations grow over time, leading to an unstable equilibrium. If some eigenvalues have zero real parts while others have negative real parts, the stability depends on higher-order nonlinear terms, requiring a more detailed analysis. Solving $\det(\lambda - JI) = 0$ gives the characteristic equation, $\prod(\lambda_i - a_i)=0$ for $i = 1,2, \dots ,8$, where a_i are the diagonal elements of J, corresponding to system parameters. For stability, all ai must satisfy, $Re(\lambda_i) < 0$. Each equation must be analyzed separately based on the system's physical constraints.

To confirm global stability, we define a Lyapunov function,

$$V(x) = \frac{1}{2}\sum x_i^2 \tag{4.3}$$

Differentiating along system trajectories,

$$V'(x) = \frac{1}{2}\sum x_i x_i' \tag{4.4}$$

Substituting system equations, we find

$$V'^{(x)} = -\frac{1}{2}c_i x_i^2 \tag{4.5}$$

where $c_i > 0$ (system-dependent parameters). Since V (x) < 0, the system is globally stable.

5. Numerical Simulation

The analysis of the propulsion system's dynamics is illustrated in the Figure 5.5 through various graphical representations, providing insights into its stability, re sponse, and energy flow. The Bode plots assess the frequency response of the DC motor, where the magnitude plot indicates high gain at low frequencies, ensuring effective disturbance rejection, while attenuation at higher frequencies minimizes in stability. The phase plot highlights increasing system lag with frequency, identify ing a critical crossover region that impacts stability. These characteristics aid in designing control mechanisms, such as PID controllers, to maintain smooth motor operation. The eigenvalue analysis of the Jacobian matrix further supports stability assessment, revealing predominantly negative eigenvalues that confirm the system's ability to return to equilibrium after small perturbations. This ensures a controlled and predictable performance of the motor, battery, and overall power distribution. Additionally, the time series plot of battery voltage and motor speed demonstrates the energy dynamics within the system. Initially, the battery voltage declines due to power consumption before stabilizing, while motor speed follows a delayed increase, reflecting the energy transfer process.

This behavior is crucial for optimizing battery management and preventing sudden power losses. Collectively, these findings confirm that the propulsion system operates within a stable regime, effectively managing power distribution while maintaining reliable performance across varying conditions. The four graphs in the Figure 5.6 provide a comprehensive analysis of the dynamic behavior and stability characteristics of a DC motor system. The first two graphs rep resent the bode magnitude and phase plots, which are essential for frequency domain analysis.

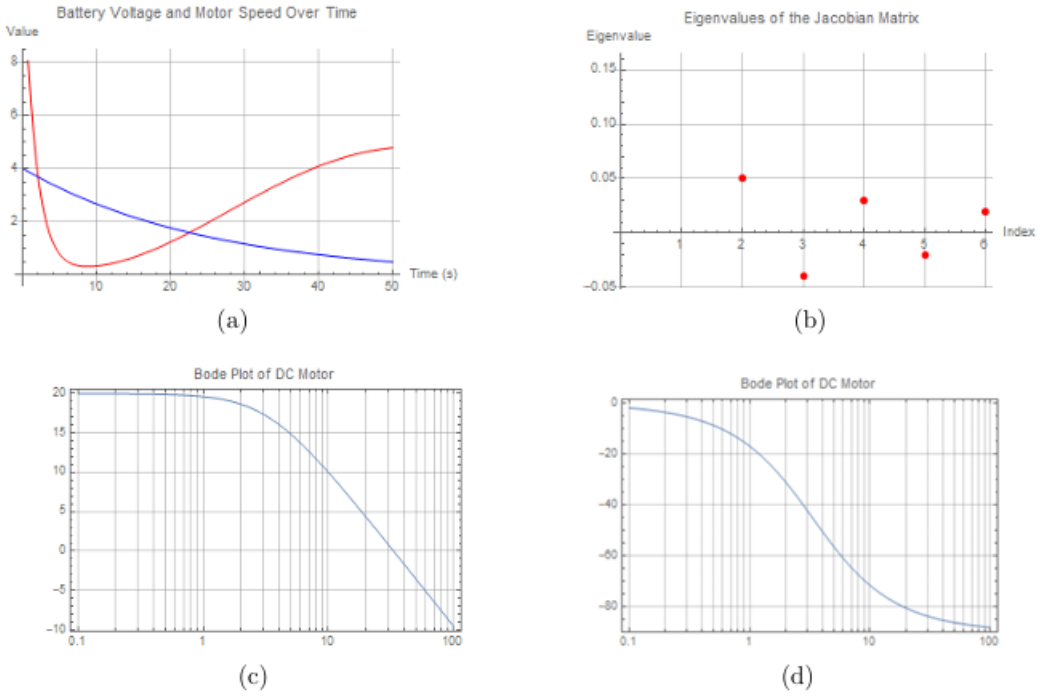

Figure 5.5: (a) represents battery voltage and motor speed interaction (b) represents the eigenvalues plot of the Jacobian matrix (c) and (d) represents the bode plot of DC motor with the values α = 0.05, β_1 = 12, γ_1= 0.02, γ_2 = 0.1, δ_1 = 0.8, δ_2 = 1.05, η = 1.12, ϵ = 0.1, γ_3 = 0.03, ψ = 0.1, λ_1 = 0.02, λ_2 = 1.5, θ = 0.04, k = 0.02, μ = 0.1.

The magnitude plot illustrates how the system's gain varies with frequency, indicating a low-pass system that effectively responds to low-frequency inputs while attenuating high-frequency noise. The phase plot, on the other hand, shows the phase shift introduced by the system, which becomes increasingly negative at higher frequencies, signifying a lag in response. These plots are crucial for designing con trollers such as PID controllers to ensure system stability. The third graph displays the eigenvalues of the Jacobian matrix, which determine the stability of equilibrium points. Positive eigenvalues indicate instability, where small perturbations grow over time, while negative eigenvalues signify a stable system where perturbations decay. A mix of positive and negative eigenvalues suggests the presence of both stable and unstable regions, requiring further analysis to determine overall system behavior. This eigenvalue analysis is particularly useful for studying nonlinear systems and de signing control strategies. The final graph presents the time-domain response of the system, showing the evolution of battery voltage and motor speed over time. The red curve, likely representing motor speed, initially decreases before rising and stabiliz ing, indicating a transient response with underdamped oscillations. The blue curve, representing battery voltage, gradually declines as energy is consumed. This analysis provides insights into energy efficiency, transient behavior, and system performance under varying conditions. Collectively, these graphs offer a detailed evaluation of the DCmotor's response in both the frequency and time domains, facilitating the develop ment of effective control mechanisms, optimizing system performance, and ensuring stability in practical applications such as robotics, electric vehicles, and industrial automation.

The four graphs collectively illustrate the frequency and time-domain behavior of a DC motor system, providing insights into its stability, response characteristics, and dynamic performance in the Figure 5.7. The first two graphs represent the Bode magnitude and phase plots, which describe how the system responds to different fre quency inputs. The magnitude plot indicates that the system behaves as a low-pass f ilter, allowing low-frequency signals while attenuating high-frequency components. The phase plot shows the phase shift introduced by the system, which becomes in creasingly negative with frequency, indicating a time lag in response. These plots are crucial for assessing the stability and control of the motor system. The third graph presents the eigenvalues of the Jacobian matrix, which determine the local stability of the system. The presence of both positive and negative eigenvalues

suggests a mix of stable and unstable regions, indicating that the system's response depends on initial conditions and system parameters. The final graph illustrates the time-domain be havior of battery voltage and motor speed. The red curve, likely representing motor speed, initially decreases before gradually rising, while the blue curve, representing battery voltage, steadily declines. This suggests a transient response where the system stabilizes over time, reflecting the energy consumption and performance characteris tics of the DC motor. Together, these graphs provide a comprehensive understanding of the motor's operational dynamics, aiding in system optimization and controller design.

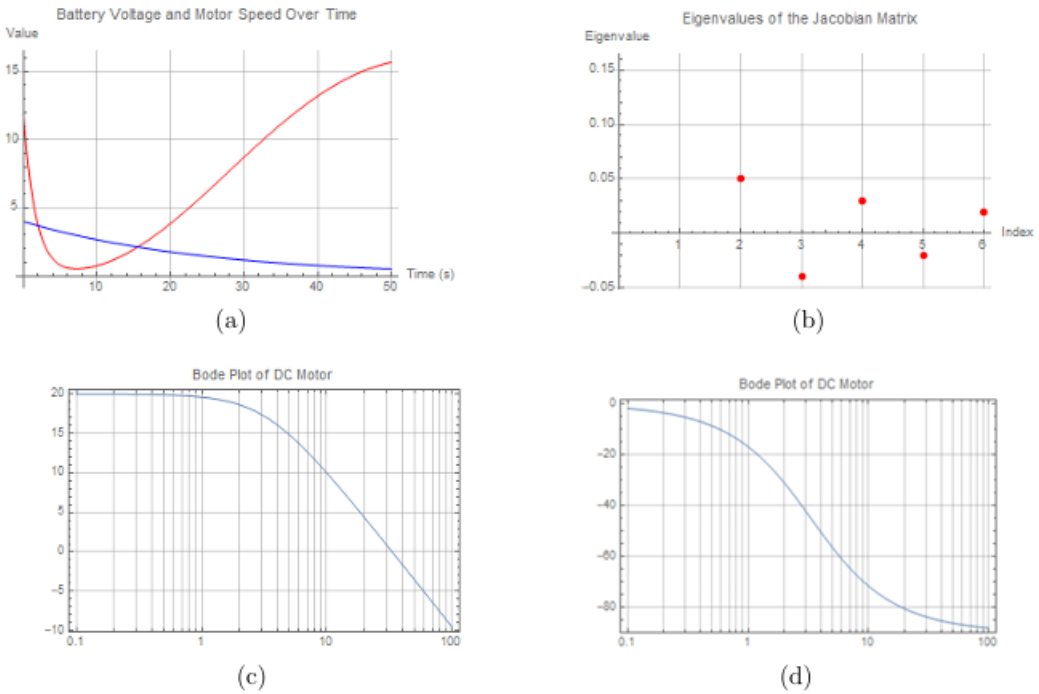

Figure 5.6: Figure (a) illustrates the interaction between battery voltage and motor speed; graph (b) illustrates the Jacobian matrices' eigenvalues; and graphs (c) and (d) illustrate the bode plot of the DC motor with the indicated values. $\alpha = 0.05$, $\beta_1 = 12$, $\gamma_1 = 0.02$, $\gamma_2 = 0.1$, $\delta_1 = 0.8$, $\delta_2 = 0.05$, $\eta = 1.12$, $\epsilon = 1.01$, $\gamma_3 = 0.03$, $\psi = 0.1$, $\lambda_1 = 1.22$, $\lambda_2 = 1.5$, $\theta = 0.04$, $k = 0.02$, $\mu = 0.1$.

The four graphs collectively illustrate the frequency response, stability, and time domain behavior of a DC motor system. The first two graphs in the Figure 5.8 represent the Bode magnitude and phase plots, which characterize the system's fre quency response. The magnitude plot shows that the system behaves as a low-pass f ilter, allowing low-frequency signals to pass while attenuating higher frequencies. The phase plot indicates the phase shift introduced by the system, which increases negatively as the frequency increases, representing the inherent time lag in response. These frequency response characteristics are essential for evaluating the stability and control performance of the motor. The third graph presents the eigenvalues of the Jacobian matrix, which determine the local stability of the system. The distribution of positive and negative eigenvalues suggests the presence of both stable and unstable regions, influencing the motor's dynamic behavior under different conditions. The f inal graph shows the time-domain response of battery voltage and motor speed over time. The red curve, which likely represents motor speed, exhibits an initial peak followed by a gradual stabilization, while the blue curve, representing battery volt age, steadily declines. This behavior reflects the transient and steady-state response of the motor, highlighting the system's energy consumption and performance over time. These analyses provide a comprehensive understanding of the motor's dynamic characteristics, contributing to improved design and control strategies.

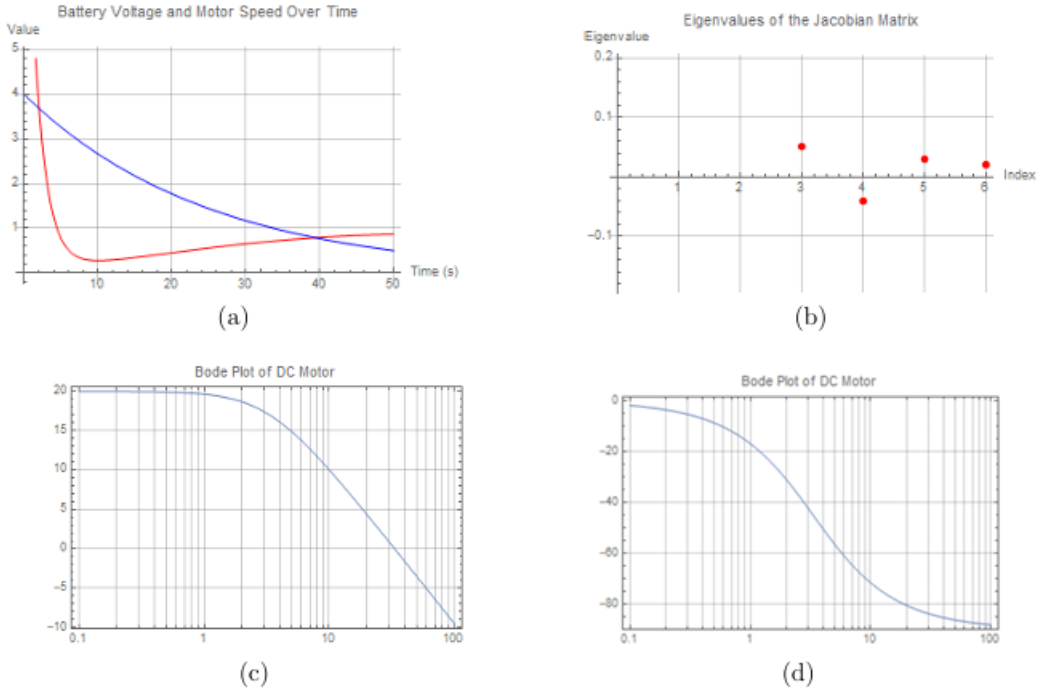

Figure 5.7: The graph in (a) illustrates the interaction between battery voltage and motor speed; the graph in (b) illustrates the Jacobian matrix's eigenvalues; the graph in (c) and (d) shows the bode plot of the DC motor with the indicated values; $\alpha = 0.05, \beta_1 = 12, \gamma_1 = 0.02, \gamma_2 = 0.1, \delta_1 = 0.8, \gamma_2 = 0.05, \eta = 1.12, \epsilon = 0.1, \gamma_3 = 0.03, \psi = 0.1, \lambda_1 = 0.02, \lambda_2 = 1.5, \theta = 0.04, k = 0.02, \mu = 0.1$.

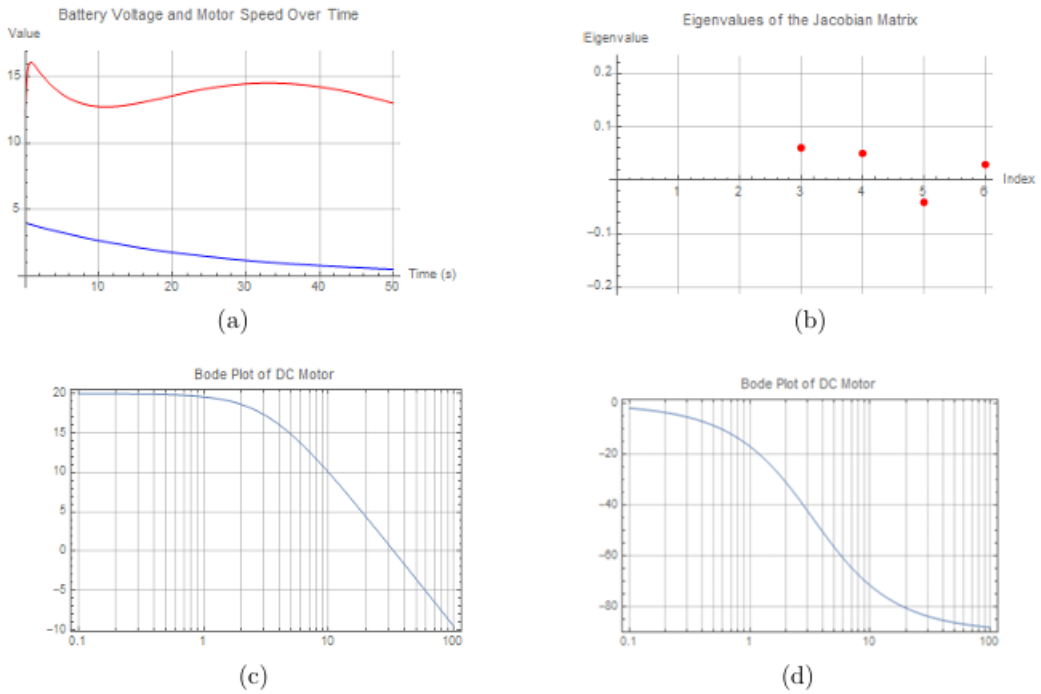

Figure 5.8: In figure (a) we illustrate the interactions between the battery voltage and motor speed; in graph (b) we illustrate the eigenvalues of the Jacobian matrix, and in graphs (c) and (d) we illustrate the bode plot of a DC motor with the indicated voltages; $\alpha = 0.05, \beta_1 = 12, \gamma_1 = 0.02, \gamma_2 = 0.1, \delta_1 = 0.8, \delta_2 = 0.05, \eta = 1.12, \epsilon = 0.1, \gamma_3 = 0.03, \psi = 0.1, \lambda_1 = 0.02, \lambda_2 = 1.5, \theta = 0.04, k = 0.02, \mu = 0.1$.

6. Discussion

Analyzing the DC motor system in terms of frequency response, stability, and time-domain behavior provides several important insights [21]. The Bode magni tude and phase plots indicate that the system acts as a low-pass filter, permitting low-frequency signals while attenuating higher frequencies. Additionally, the phase response indicates that stability and control are affected by an increasing time lag with frequency. According to the Jacobian matrix, there is a combination of stable and unstable regions, revealing the system's dependence on its initial conditions and parameter values [15], [18] and [19]. Furthermore, the time-domain response of the battery voltage and motor speed shows an initial transient phase prior to stabilization, illustrating the evolution of energy consumption over time and the performance of the system. These findings contribute to a deeper understanding of the operation of DC motors, thereby facilitating system optimization and the development of efficient and effective controllers to improve their performance and stability.

Conflict of Interest

There is no conflict of interest among the authors.

References

[1] M. Aakash, C. Gunasundari, Mutum Zico Meetei, H. Ahmed Msmali, Fractional Order Mathematical Modelling of HFMD Transmission via Caputo Derivative, Axioms 13(4) (2024). DOI:10.3390/AXIOMS13040213.
[2] M. Becherif, M.Y. Ayad, A. Djerdir, A. Miraoui, Electrical train feeding by association of supercapacitors, photovoltaic and wind generators, In Proceedings of IEEE-ICEE, Capri-Italy (2007) 55-60.
[3] M.B. Camara, H. Gualous, F. Gustin, A. Berthon, Control strategy of Hybrid sources for Transport applications using supercapacitors and batteries, In Power Electronics and Motion Control Conference, IPEMC APOS06, CES/IEEE 5th International Vol (1) 14-16 (2006) 1-5.
[4] C. Lungoci, E. Helerea, A. Munteanu, On a energy supply combined system used in electric vehicle, In Bulletin of the Transilvania University of Brasov, Vol. 13 (48) (2006) 213-218.
[5] A. Lungoci, M. Becherif, A. Miraoui, E. Helerea, On board energy system based on batteries and supercapacitors, In Proceedings of Convergence of Information Technologies and Control Methods with Power Plants and Power Systems ICPS IFAC'07, Cluj-Napoca, (2007) 197-202.
[6] M.D. Tinney, J. Hensler, Efficiency and Power Density Improvements in Electric Propulsion Systems, In INEC 94 Cost Effective Maritime Defence, The Institute of Marine Engineers (1992) 23-52.
[7] P.H. Sallabank, A.J. Whitehead, The Practical Application of Modern Simula tion Tools Throughout the Designa and Trials of a Diesel Electric Propulsion System, Trans ImarE 107 (1995) 101-117.
[8] W.W. Price, H.D. Chiang, H.K. Clark, C. Concordia, D.C. Lee, J.C. Hsu, S. Ihara, C.A. King, C.J. Lin, Y. Mansour, K. Srinivasan, C.W. Taylor, E. Vaa hedi, Load Representation for Dynamic Performance Analysis IEEE Task Force Report, IEEE Trans., Power System 8(2) (1993) 472-482. 16
[9] M. Aakash, C. Gunasundari, S. Sabarinathan, Salah Mahmoud Boulaaras, Ahmed Himadan, Mathematical insights into the SEIQRD model with allee and fear dynamics in the context of COVID-19, Partial Differential Equations in Applied Mathematics 11 (2024) DOI:10.1016/j.padiff.2024.100756.
[10] G. Santhosh Kumar, C. Gunasundari, Analysis of two prey and one predator interaction model with discrete time delay, Asia Pacific Academic 10(28) (2023) 10-28.
[11] A. Sciarretta, L. Guzzella, Vehicle propulsion systems: introduction to modeling and optimization (2005).
[12] J.M. Miller, Propulsion systems for hybrid vehicles Vol 45 (2004) Iet.
[13] M. Vidyasagar, Nonlinear systems analysis, Society for Industrial and Applied Mathematics (2002).
[14] G. Santhosh Kumar, C. Gunasundari, Dynamical analysis of two-preys and one predator interaction model with an Allee effect on predator, Malaysian Journal of Mathematical Sciences 17(3) (2023) 263-281.
[15] T. M. Wetterhus, Comparison of fuel consumption in electric propulsion systems with fixed speed and variable speed thruster motors. Master's thesis, Norwegian Institute of Technology, Department of Electric Power Engineering (1995).

[16] M. Aakash, C. Gunasundari, Analysis of fractional order mathematical mod elling of HFMD transmission via ABC derivative, Mathematica Applicanda, 51(2) (2023) DOI:https://doi.org/10.14708/ma.v51i2.7229.
[17] G. Santhosh Kumar, C. Gunasundari, Turing instability of a diffusive predator prey model along with an Allee effect on a predator, Commun. Math. Biol. Neurosci., (2022) Article ID 40.
[18] H.G. Kwatny, C. Maffezzoni, J. J. Paserba, J.J. Sanchez-Gasca, E.V. Larsen, The Control Handbook, CRC Press, ch. 79, Control of Electrical Power (1996) 1453-1495.
[19] T.I. Fossen, Guidancea, Control of Ocean Vehicles, Wiley (1994).
[20] A. Choucha, S.M. Boulaaras, D. Ouchenane, B.B. Cherif, M. Abdalla, Exponen tial stability of swelling porous elastic with a viscoelastic damping and distributed delay term, Journal of Function Spaces 2021(1) (2021) 5581634.
[21] S. Alqahtani, M. Iqbal, A.R. Seadawy, Y. Jazaa, A.A. Rajhi, S.M. Boulaaras, E.A. Az-Z´ obi, Analysis of mixed soliton solutions for the nonlinear Fisher and diffusion dynamical equations under explicit approach, Optical and Quantum Electronics 56(4) (2024) 647.

G. Santhosh Kumar is an Assistant Professor in the Department of Mathematics, Easwari Engineering College, Ramapuram, Chennai. He has completed his M.Sc. Mathematics from the Madras University in 2019 and Ph.D., from SRM University in 2025. His main research interests are mathematical biology. He has co-authored more than 7 research papers (31+ Google Citations with h-index 4), (16+ Scopus Citations with h-index 2).

Aakash Mohandoss is an Assistant Professor in the Department of Mathematics, Jeppiaar Engineering College, Jeppiaar Nagar, Chennai. He has completed his M.Sc., in 2021 and Ph.D., in 2024 from SRM University, Kattankulathur. His main research interests are mathematical modelling and differential equations. He has co-authored more than 10 research papers (65+ Google Citations with h-index 4), (40+ Scopus Citations with h-index 3).